NAVAL POSTGRADUATE SCHOOL

MONTEREY, CALIFORNIA

THESIS

ANALYSIS OF PRACTICAL EMPLOYMENT OF DRAG ENHANCED DE-ORBITING DEVICES FOR MIDSIZED LEO SATELLITES

by

Adam Fuller

June 2021

Thesis Advisor: Jennifer L. Rhatigan
Co-Advisor: Daniel J. Sakoda

THIS PAGE INTENTIONALLY LEFT BLANK

REPORT DOCUMENTATION PAGE			*Form Approved OMB No. 0704-0188*

1. AGENCY USE ONLY *(Leave blank)*	**2. REPORT DATE** June 2021	**3. REPORT TYPE AND DATES COVERED** Master's thesis

4. TITLE AND SUBTITLE ANALYSIS OF PRACTICAL EMPLOYMENT OF DRAG ENHANCED DE-ORBITING DEVICES FOR MIDSIZED LEO SATELLITES	**5. FUNDING NUMBERS**
6. AUTHOR(S) Adam Fuller	
7. PERFORMING ORGANIZATION NAME(S) AND ADDRESS(ES) Naval Postgraduate School Monterey, CA 93943-5000	**8. PERFORMING ORGANIZATION REPORT NUMBER**
9. SPONSORING / MONITORING AGENCY NAME(S) AND ADDRESS(ES) N/A	**10. SPONSORING / MONITORING AGENCY REPORT NUMBER**

11. SUPPLEMENTARY NOTES The views expressed in this thesis are those of the author and do not reflect the official policy or position of the Department of Defense or the U.S. Government.

12a. DISTRIBUTION / AVAILABILITY STATEMENT Approved for public release. Distribution is unlimited.	**12b. DISTRIBUTION CODE** A

13. ABSTRACT (maximum 200 words)

The use of drag-enhancing devices for satellite de-orbit has been successfully demonstrated on small satellites, and analysis shows they can be a practical method for de-orbiting many midsized low-earth orbit (LEO) satellites. A satellite's mass, orbital regime, ballistic coefficient, and other characteristics delineate the techniques and trade-offs related to implementing a drag device as a de-orbiting tool. In addition to reviewing the successes of drag devices to date in de-orbited spacecraft, Rhatigan and Lan outlined the trade space available for expansion of this technology to a large range of midsize spacecraft. This study examines that trade space in more detail and with a wide span of existing midsized LEO satellites. Through the analysis of these satellite characteristics and orbital regimes, this study suggests that the potential for fuel mass savings exists for a significant percentage of the midsized satellites. Furthermore, satellites that would still require some propulsion to de-orbit within 25 years show similar fuel mass savings. Drag-enhancing device requirements driven by this study are shown to be achievable within the scope of existing prototypes and realistic drag device designs.

14. SUBJECT TERMS drag, drag device, drag enhancement, drag sail, satellite, orbital debris, medium-sized satellite, LEO satellite, de-orbit, ballistic coefficient	**15. NUMBER OF PAGES** 69
	16. PRICE CODE

17. SECURITY CLASSIFICATION OF REPORT	**18. SECURITY CLASSIFICATION OF THIS PAGE**	**19. SECURITY CLASSIFICATION OF ABSTRACT**	**20. LIMITATION OF ABSTRACT**
Unclassified	Unclassified	Unclassified	UU

NSN 7540-01-280-5500

Standard Form 298 (Rev. 2-89)
Prescribed by ANSI Std. 239-18

THIS PAGE INTENTIONALLY LEFT BLANK

Approved for public release. Distribution is unlimited.

ANALYSIS OF PRACTICAL EMPLOYMENT OF DRAG ENHANCED DE-ORBITING DEVICES FOR MIDSIZED LEO SATELLITES

Adam Fuller
Major, United States Marine Corps
BS, University of Wisconsin – Whitewater, 2008

Submitted in partial fulfillment of the
requirements for the degree of

MASTER OF SCIENCE IN SPACE SYSTEMS OPERATIONS

from the

NAVAL POSTGRADUATE SCHOOL
June 2021

Approved by: Jennifer L. Rhatigan
Advisor

Daniel J. Sakoda
Co-Advisor

James H. Newman
Chair, Space Systems Academic Group

THIS PAGE INTENTIONALLY LEFT BLANK

ABSTRACT

The use of drag-enhancing devices for satellite de-orbit has been successfully demonstrated on small satellites, and analysis shows they can be a practical method for de-orbiting many midsized low-earth orbit (LEO) satellites. A satellite's mass, orbital regime, ballistic coefficient, and other characteristics delineate the techniques and trade-offs related to implementing a drag device as a de-orbiting tool. In addition to reviewing the successes of drag devices to date in de-orbited spacecraft, Rhatigan and Lan outlined the trade space available for expansion of this technology to a large range of midsize spacecraft. This study examines that trade space in more detail and with a wide span of existing midsized LEO satellites. Through the analysis of these satellite characteristics and orbital regimes, this study suggests that the potential for fuel mass savings exists for a significant percentage of the midsized satellites. Furthermore, satellites that would still require some propulsion to de-orbit within 25 years show similar fuel mass savings. Drag-enhancing device requirements driven by this study are shown to be achievable within the scope of existing prototypes and realistic drag device designs.

THIS PAGE INTENTIONALLY LEFT BLANK

TABLE OF CONTENTS

THIS PAGE INTENTIONALLY LEFT BLANK

LIST OF FIGURES

THIS PAGE INTENTIONALLY LEFT BLANK

LIST OF TABLES

LIST OF ACRONYMS AND ABBREVIATIONS

a	semi-major axis
ANDE	Atmospheric Neutral Density Experiment
CALIPSO	Cloud-Aerosol Lidar and Infrared Pathfinder Satellite Observations
C_B	ballistic coefficient
C_D	coefficient of drag
CNES	Centre National d'Études Spatiales
DAS	debris assessment software
DMSP	Defense Meteorological Space Program
e	eccentricity
e	Euler's number
EO-1	Earth Observation 1
EOL	end-of-life
ERS-1	European Remote-Sensing Satellite -1
ESA	European Space Agency
FY-1	FengYun-1
g_o	standard gravity
h	height
HST	Hubble Space Telescope
i	inclination
IRS-P4	OceanSat-1 - formerly IRS-P4 (Indian Remote Sensing Satellite -P4)
I_{sp}	specific impulse
kg	kilograms
km	kilometers
LEO	low-earth orbit
ln	natural log
M	mean anomaly
m	meters
m_f	final total mass
m_o	initial total mass
NASA	National Aeronautics and Space Administration

NPSAT-1	Naval Postgraduate School (NPS) Spacecraft Architecture and Technology Demonstration Satellite
NRL-MSISE-00	Naval research Laboratory Mass Spectrometer and Incoherent Scatter Radar, "E" model
OCO-2	Orbiting Carbon Observatory-2
ODMSP	Orbital Debris Mitigation Standard Practices
ORDEM	NASA Orbital Debris Engineering Model
r	radius
r_a	radius of apogee
r_p	radius of perigee
s	side length
SA	surface area
SRP	solar radiation pressure
STELA	Semi-analytic Tool for End of Life Analysis software
TLE	two-line elements
TUI	Tethers Unlimited, Incorporated
μ	earth gravitational constant
v_a	velocity at apogee
ve	exhaust velocity
v_p	velocity at perigee
w	width
Z_a	apogee geocentric altitude
Z_p	perigee geocentric altitude
ΔV	change in velocity
ω	argument of periapsis
Ω	right ascension of the ascending node
π	pi

ACKNOWLEDGMENTS

I would like to acknowledge and thank my advisors, Dr. Jennifer Rhatigan and Dan Sakoda, for their mentorship, enthusiasm, and countless hours dedicated toward this work. Additionally, I express my gratitude to all the faculty at Naval Postgraduate School to include the Graduate Writing Center, the Thesis Processing Office, and all the instructors over the past two years who have helped to provide me with an outstanding education. Finally, to my wife, Leslie, and two daughters, Alice and Lucy. I appreciate all your sacrifices and support always, but particularly over this past pandemic-stricken and difficult year for us all.

THIS PAGE INTENTIONALLY LEFT BLANK

I. INTRODUCTION

A. OVERVIEW

Drag-enhancing de-orbiting devices for midsized[1] satellites have been shown to have practical advantages; however, specific satellites and their characteristics have not been thoroughly analyzed to fully understand the concept of operations, trade-offs, and design requirements. This study focuses on the application of drag-enhancing technologies to midsized LEO satellites, a class of satellite expected to grow substantially [1]. The examination includes a wide span of existing midsized satellites using realistic characteristics such as ballistic coefficients, orbital parameters, and masses to determine both the practicality of implementing a drag device as well as to identify an approach or concept of operations for each satellite.

The first part of this study examines and validates the primary software tool used in the analyses, the *Semi-analytic Tool for End of Life Analysis* (STELA) software version 3.3. STELA is a tool developed by the Centre National d'Études Spatiales (CNES) to estimate the de-orbit intervals for satellites. The software uses a satellite's orbital parameters, satellite specifications, and an atmospheric model to estimate orbit decay times. The satellite specifications include the total mass and drag area of the spacecraft. Validation case studies were conducted to ensure consistency with results from the similar NASA Debris Assessment Software (DAS) and with known de-orbit times of satellites that have decayed. This lends confidence to later decay predictions and allows insight into the limitations of these estimates.

A set of satellites chosen to span a large range within the "midsized" designation provides the data set for this study. Analyses conducted on this data set are consistent with the previously validated approach using STELA. While the general trade-space was predicted by [2] and [3], this study tests those predictions with data from actual satellites

[1] Midsized refers to satellites approximately 500–1000 kg in mass. Details of why this regime is targeted is explained later.

in orbit. The analyses of this data can then be used to further the design of practical drag devices.

To develop a concept of operations for the implementation of drag devices, certain assumptions with respect to spacecraft dimensions, effective cross-sectional areas, and drag coefficients were necessary. Limitations in this study, primarily due to model uncertainties such as unpredictable atmospheric conditions, potential spacecraft tumbling, estimations of drag coefficients, and satellite areas, are discussed in detail. Since both STELA and DAS are estimating tools, the intent is not to perfect the estimations, but to achieve enough accuracy and consistency to draw conclusions on trends for the analyses. Predicting orbital decay is extremely complex, and it is highly driven by the particulars of a given solar cycle. Using generally accepted models of past solar cycles is perhaps the largest source of uncertainty. Within this constraint, it is important to ensure that the analyses are accurate enough to provide realistic data to further define the practicality of drag enhancing devices. The modeling approach uses some simplification, to be explained further, such as determining surface areas or propulsion systems specifications.

Following the determination of a modeling approach, a range of existing "midsized" satellites was collected for the analyses, spanning masses from 442 kg to 1050 kg. Each satellite was then modeled in STELA with current orbital parameters, gathered from their respective two-line elements (TLE) from SpaceTrack.org [4]. Natural de-orbit times were estimated, and then new de-orbit times were estimated for different scenarios of drag enhancing devices to determine both the practicality and possible methods of utilizing such a device.

This thesis demonstrates a wide variety of useful applications of drag-enhancing devices on midsized satellites. Many of the spacecraft in this study could have met current de-orbit times within the necessary 25-year limit simply by deploying a drag device with a reasonable and achievable deployed area. These satellites, as well as others, could achieve fuel savings with a drag device. Current prototypes and pre-existing drag devices show promise for future medium-sized spacecraft.

B. BACKGROUND AND PREVIOUS STUDIES

This study stems from orbital debris mitigation efforts. In 2001, the U.S. government established the Orbital Debris Mitigation Standard Practices (ODMSP) [5] to "address the increase in orbital debris in the near-Earth space environment." Current U.S. regulations specify that spacecraft shall be passivated and safely disposed of at the end-of-life (EOL). Specifically, the following regulation applies to U.S. spacecraft in low-earth orbit (LEO). ODMSP [5] states,

> Atmospheric reentry: Leave the structure in an orbit in which, using conservative projections for solar activity, atmospheric drag will limit the lifetime to as short as practicable but no more than 25 years after completion of mission. If drag enhancement devices are to be used to reduce the orbit lifetime, it should be demonstrated that such devices will significantly reduce the area-time product of the system or will not cause spacecraft or large debris to fragment if a collision occurs while the system is decaying from orbit.

Additionally, it is notable that recently adopted international guidelines recommend de-orbit within 25 years of the *beginning of life* [6].

Despite these regulations, adherence to such policies is limited. Planned compliance is a prerequisite required for launch approval [5]. However, carrying out the de-orbit plan is left to the operator and therefore remains susceptible to deviations. Furthermore, space traffic management authorities do not possess the ability to control or influence a spacecraft once it is in orbit. Often enough, the decision to use onboard fuel to extend a satellite's life as opposed to de-orbiting as planned will be in the interest of the satellite's owner. One such case was Earth Observation 1 (EO-1), which used its remaining de-orbit fuel to extend its mission life [7]. This resulted in an expected reentry time well beyond the 25-year regulation [3]. For these reasons, passive devices such as a drag mechanism may provide a practical solution because they remove the ability to depart from the intended usage of onboard fuel—or, as stated in [3], "single-purpose drag devices force compliance." Nevertheless, the inclusion of a drag device does not provide a free solution to debris mitigation, and design requirements are paramount to the effectiveness of their use. Therefore, the design must consider the possible trade-offs that are available to the operator, such as fuel mass savings and extended operational lifetime versus increased

complexity and mass of the additional device [2]. This motivates adherence to design principles, outlined later in this section, so that these devices are most attractive for implementation by designers and operators.

This section addresses previous research to provide a background on drag device examples and analysis. It explains how the combination of ballistic coefficients and orbital altitudes identify the effective employment regime for the use of drag devices. Additionally, it introduces the design guidelines and requirements that are necessary towards solving the problem statement outlined below.

The ballistic coefficient is defined below, where m is the spacecraft's mass, A is the effective cross-sectional area and C_D is the drag coefficient [8]. The ballistic coefficient is a component of the drag force on a satellite, along with atmospheric density.

$$C_B = \frac{m}{A \cdot C_D} \tag{1}$$

The introduction of a drag device, in effect, is a change in the spacecraft's area, and thus its ballistic coefficient. A decrease in C_B at (EOL) accelerates the satellite's orbital decay, thereby removing it as a debris threat to other satellites.

Notably, this increased cross-sectional area also could affect the area-time product ($A \bullet t$), where A is the effective cross-sectional area and t is time, discussed in [5]. The area-time product in the ODMSP is a proxy for risk: reducing $A \bullet t$ reduces risk of debris production. Risk reduction can also be accomplished by minimizing the potential for debris production in design (e.g., drag devices are often composed of lightweight, flexible "sail" material which may tear, rather than fragment, as a result of collision). The analyses in this study show that the area-time product is decreased for most of the spacecraft examined, although some of those scenarios may not be considered "significantly reduced" [5]. Nevertheless, it is also likely that the increased drag area produced by thin, lightweight material "will not cause spacecraft or large debris to fragment if a collision occurs" [5].

An earlier work [3] reviewed the flight history of drag-enhancing devices that have been effectively used on small LEO satellites. That analysis showed that they are also practical for use on midsized satellites. Unlike larger spacecraft, small satellites have

demonstrated drag-enhancing devices for de-orbit such as NanoSail-D in 2010 [9]. Drag devices are effective for de-orbiting small satellites due to the relatively small mass, which generally yields a smaller ballistic coefficient. However, most smaller satellites (<100 kg) will de-orbit within 25 years, thus drag devices may have more value when applied to midsized satellites (500–1000 kg) that typically have a larger ballistic coefficient [1].

Rhatigan and Lan [3] showed the relationship between the ballistic coefficient and altitude for a practical regime for drag-enhancing devices (Figure 1). "Region 1 (in green) is the regime where spacecraft will naturally decay within the required time period; above this in Regions 2 and 3, spacecraft will not meet decay requirements without intervention" [2].

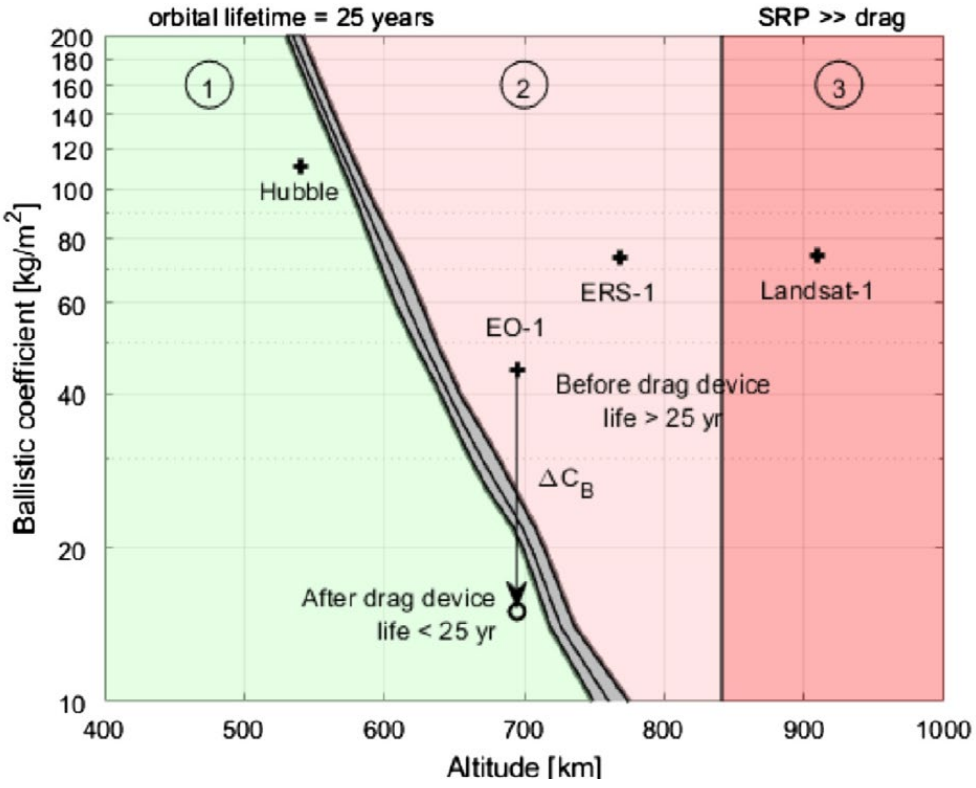

Note the wide boundary between regions 1 and 2 is representative of variations in the solar cycle.

Figure 1. Drag device effect and typical ballistic coefficient for small, midsized, and large spacecraft. Source: [3].

Figure 1 also includes some sample satellites, such as EO-1, the Hubble Space Telescope (HST), and European Remote-Sensing Satellite-1 (ERS-1). The HST will eventually de-orbit on its own [10]. In their study, altitudes above 850 km (Region 3) were not considered because the solar radiation pressure (SRP) above 850 km is the dominant force [2] and the unpredictable disturbances in SRP significantly affect the de-orbit estimations. Region 2 is the area of interest for this study because the ballistic coefficient may be lowered to achieve a decay within regulation. As shown in the figure, EO-1 is an example wherein the decrease in ballistic coefficient would have been practical since an increase of surface area of 6.09 m^2 and total surface area of 12.2 m^2 [2] is within the demonstrated capability of drag devices. However, ERS-1 is an example wherein de-orbit can be achieved in theory, but the mass of satellite (2384 kg) [11] would require a surface area more than 100 m^2, which is less practical. ERS-1 demonstrates how the effectiveness of drag devices relates to mass—where a massive satellite will require a much larger cross-sectional area increase to lower the ballistic coefficient. Additionally, one can see from Figure 1 that to de-orbit within 25 years, satellites at a higher altitude require a greater decrease in ballistic coefficient (compared to the same satellite at a lower altitude). In some cases, an alternative strategy may be required, such as an initial de-orbit burn followed by employment of a drag device for de-orbit. This is explored later as a trade-study.

C. PROBLEM STATEMENT

This study seeks to explore Region 2 within this figure via practical study of real spacecraft examples using orbital altitudes, mass, and de-orbit strategies to determine drag device requirements and practical application of drag devices. This study examines current satellites that fall within the midsized range (approx. 500–1000 kg) and applies strategies for de-orbit that can optimize costs and ultimately refine design requirements for future drag devices. From the examination and analysis of midsized satellites, it becomes clearer where realistic limitations exist for a workable drag de-orbiting device.

The benefits of drag devices also have the potential to go beyond simply debris mitigation. As mentioned in [2], some additional benefits could include mass savings, extended operational lifetime, or “greater tolerance to attitude determination and control

failures." Aside from potential benefits, certain design guidelines are also spelled out in [3] that facilitate a device to be feasible, reliable, and overall acceptable to be put into practice. These include:

- The device should avoid interfering with the primary mission. The device should remain stowed until commanded to release. To avoid inadvertent release, at least a single-fault tolerant release should be considered.
- The drag area should be sufficient to de-orbit the spacecraft within 25 years using standard de-orbit calculation tools (e.g., STELA or DAS). If the mission permits, consider an earlier disposal, taking advantage of the solar cycle (Section 2.2 of Rhatigan and Lan) [3].
- Since deployment occurs at EOL, this action, and any commanding of it, should be highly reliable, in keeping with the mission reliability requirements. Sufficient testing to assure reliability should be included in the test plan.
- The mass of the de-orbit device should be minimized. A reasonable mass target is the mass of the propellant displaced for a de-orbit maneuver if the de-orbit device were not included.
- The de-orbit device is expected to operate at the spacecraft EOL and survive to the entry interface altitude, so materials should be selected to endure the corrosive LEO environment (i.e., atomic oxygen attack, ultra-violet radiation degradation and micrometeoroids and orbital debris).
- The device should be simple to integrate and operate. The pyramid configuration is favored for small spacecraft that have one side to dedicate to the de-orbit device. Modular designs are favored for more complex spacecraft that may not have a single location available but could accommodate de-centralized sail areas.

The purpose of these guidelines allows this analysis to form realistic boundaries of what can and cannot be expected to take place. Later in this study, these guidelines will be used to evaluate individual case studies to determine where feasible design requirements overlap with the necessary functionality of de-orbiting midsized satellites.

II. SIMULATION AND VALIDATION OF MODELING SOFTWARE

The primary software used in this study to predict satellite de-orbit is STELA [12]. Additionally, this study used the DAS [13] to validate results from STELA and ensure consistency. To better understand the uncertainties associated with de-orbit prediction, it was necessary to examine STELA, validate its accuracy and determine the effects of assumptions or unknowns that were used throughout this analysis. The first part of this process includes a brief overview of STELA and DAS. Secondly, STELA predictions were compared to data from two-line elements (TLEs) of decayed satellites to validate and compare to results in DAS. Spherical satellites were chosen for this validation phase to minimize the effects of area calculations and simplifications. Finally, these case studies and the history of other such research are used to assess the uncertainties for the later analysis of a broader range of satellites.

A. STELA, DAS, AND TLES

STELA uses iterative computations and performs long-term propagation of satellite locations in LEO to predict atmospheric reentry duration [12]. Orbital parameters required for simulation can be derived from the spacecraft's TLEs. The primary orbital parameters that affect the decay duration are the perigee (Zp) and apogee (Za) altitudes. The other orbital parameters of inclination (i), right ascension of the ascending node (Ω), argument of perigee (ω), and mean anomaly (M) also play a factor in the orbit duration; however, they are less significant for the objectives of this study and their values are included here for reference purposes. Object characteristics include total mass, mean cross-sectional area, the reflectivity coefficient, and a drag coefficient [12]. The default and most current atmospheric model in STELA is the Naval Research Laboratory Mass Spectrometer and Incoherent Scatter Radar, "E" model (NRL-MSISE-00), which extends from Earth ground through the exosphere, released in 2000. A solar activity file is another parameter setting in STELA used to model the space environment. The solar activity variable file contains information made from daily solar flux, the mean solar flux and the geomagnetic 3-hour index [12]. The other options for solar activity include a user defined value and a "mean

constant" that uses "normalized solar activity computed from the ballistic coefficient of the spacecraft and the apoapsis altitude of the initial orbit" [12]. The solar variable activity file is used in this study because it provides the most accurate simulations when used in the validation case studies.

DAS is a similar software program that can be used to estimate the decay of satellite orbits. DAS is a "tool to aid NASA programs to perform the required mission risk analysis according to the NASA Safety Standard" [13]. Overall, the function of DAS is similar to that of STELA, and while it is not the primary software used in this thesis, it is another tool to further authenticate the analysis. STELA was chosen for this study primarily for its ease of use. STELA is publicly available while DAS is restricted, so results herein can be duplicated.

TLEs were gathered from the database SpaceTrack.org, which provides observation measurements of spacecraft. The measurements collected on satellites come from the wide array of Space Situational Awareness assets that derive a TLE, which is an estimation of a given satellite's position and orbital parameters. While this estimation is by no means a perfect depiction of true position, it nevertheless is a consistent and reliable source for the scope of this research. For the purposes of this study, the TLE data can be considered the reality of an orbit while the STELA and DAS software yields an estimation of future orbital decay. The validation case studies discussed below compare the TLE data with the estimations from both STELA and DAS.

B. VALIDATION CASE STUDIES

Since de-orbit estimation relies on the effective cross-sectional area of a satellite, it is critical to have accurate dimensions for validation. Previous studies [1] have shown that STELA tends to be conservative with respect to de-orbit predictions, meaning that the spacecraft is predicated to decay later than reality (a useful and conservative trait).

For validation purposes, satellites were chosen with known re-entry dates and with simple spherical geometry, to remove uncertainty associated with effective cross-sectional area calculations. The Atmospheric Neutral Density Experiment (ANDE) satellites

comprised a mission conducted by the Naval Research Laboratory and consisted of spherical satellites used to analyze air density and improve orbit determination [14]. These unique satellites remove one ambiguity in the calculation of the ballistic coefficient since the area and mass are known, and the shape is a nearly perfect sphere.[2] It is assumed that these passive satellites are tumbling; however, regardless of the orientation, the cross-sectional area of drag will be constant because of the spherical shape. Two of the ANDE satellites (ANDE-2 Pollux and ANDE-2 Castor) were used to validate our STELA simulations.

All the orbital parameters were taken directly from the TLE data[3] or based on the referenced satellite specifications (mass and area). However, the C_D is not usually specified and is unique to each satellite based on the geometric shape, altitude, and surface condition (e.g., specular, or reflective) [8]. The default C_D in STELA is 2.2; however, in the case of a sphere, the C_D ranges from 2 to 2.6 based on the surface condition. A C_D of 2 was used below as it yields results closer to the actual decay. The satellite specifications and initial orbital parameters are listed in Table 1.

Table 1. ANDE STELA inputs. Adapted from [4], [14].

Parameter/Satellite	**ANDE-2 Pollux**	**ANDE-2 Castor**
Mass (kg)	27.442	47.45
Area (m^2)	0.1829	0.1829
C_D	2	2
NORAD ID	35693	35694
Start date	2009-07-31	2009-07-31
z_p	328.78	328.73
z_a	333.42	334.20
i	51.64	51.64
Ω	81.34	81.34
ω	36.25	34.27
M	323.82	325.89

[2] Most midsize spacecraft have highly complex geometries, including multiple appendages (solar panels, antennae, etc.) that drive higher uncertainty in drag area estimation.

[3] The validation case studies use a TLE date shortly after the satellites are inserted into their initial orbits.

The above information was then modeled in STELA and compared to the known de-orbit dates of each satellite. Archived TLEs for the satellites were extrapolated from Spacetrack.org [4] and plotted using the semi-major axis versus the days on orbit (Figures 2 and 3). Figures 2 and 3 compare actual TLE data with the initial propagation performed with STELA for the two ANDE-2 satellites (Pollux and Castor).

As shown, this validation runs counter to the conservative trend noted earlier for STELA and predicts an earlier re-entry. There is a 43-day difference in predicted vs. actual re-entry, for a mission duration of 8 months. While 43 days is not significant relative to a 25-year de-orbit requirement, consideration must be given to be conservative elsewhere, such as in design of de-orbit devices if this predictive error is sustained.

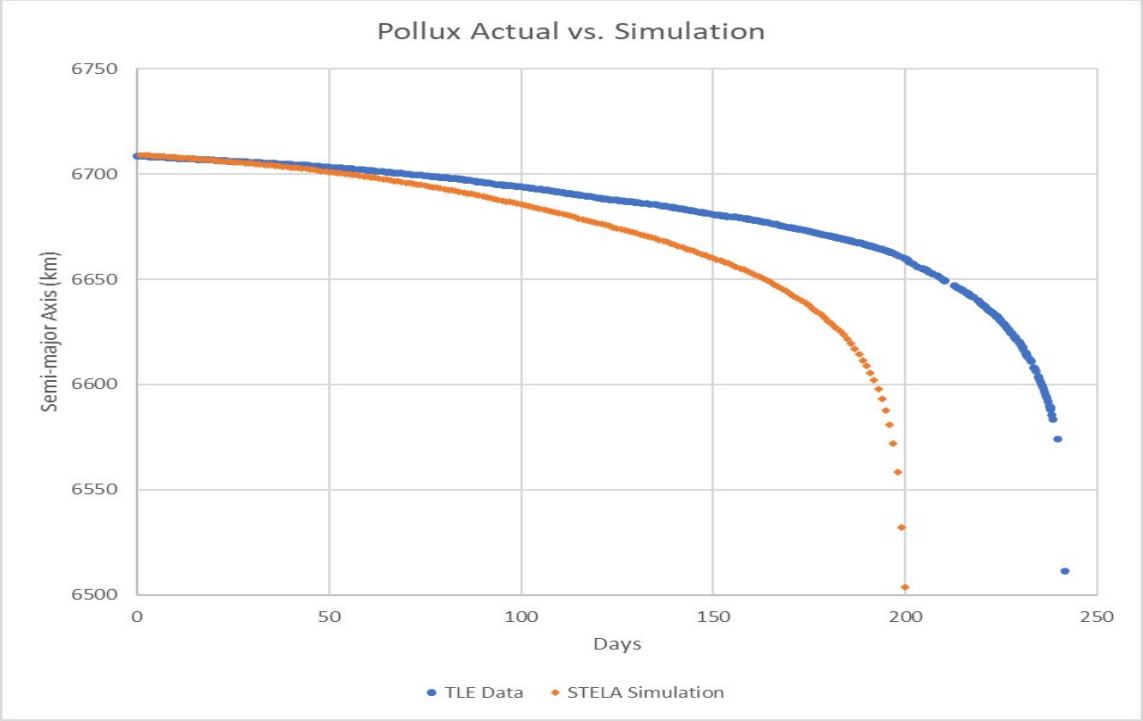

Figure 2. Orbital decay of ANDE Pollux using actual TLE versus STELA predictions.

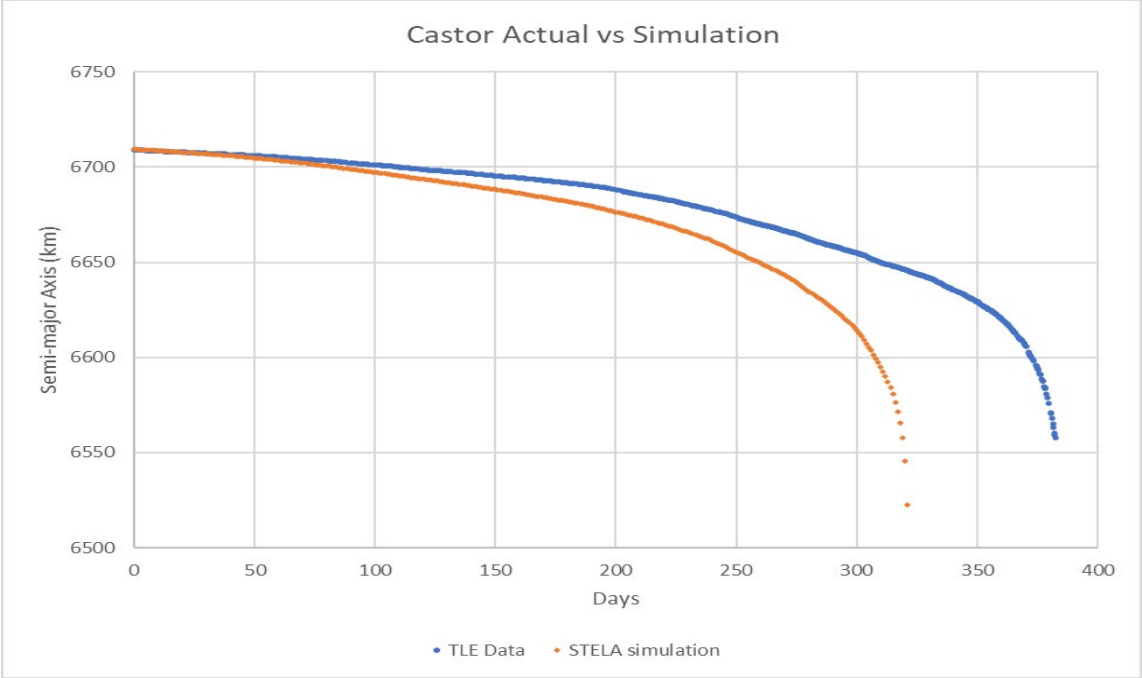

Figure 3. Orbital decay of ANDE Castor using actual TLE versus STELA predictions.

In both cases the TLEs (actual) indicate the satellite was on orbit longer than the simulation predicts from the initial orbital inputs using STELA. One possibility for this may be due to the inclination of 51°, which is within the critical inclination group as identified in STELA in the ranges 40°–80°. According to Le Fèvre et al. [15], "at these inclinations, resonance effects due to various perturbation sources (solar radiation pressure, third-body perturbation and drag in particular) have been shown to have significant effects on LEO lifetime in some cases." The recommendation for this is to decrease the integrator step and run multiple iterations; the integration step for the ANDE satellites was decreased to 6 hours, as opposed to the default 24 hours [12]. However, after multiple simulations at the reduced integrator step, the STELA results were consistent to within one day, but did not significantly improve the underestimation.

The TLEs and initial orbital data were also compared to the simulation in DAS (shown in Figures 4 and 5). The results in DAS were also less conservative than reality, but very similar to that of STELA. To further validate the results, TLEs beyond the initial

orbit start date were also modeled to determine whether the TLEs, DAS and STELA would agree on decay dates (diamond, circle, and triangle data points in Figures 4 and 5). This modeling was completed for both STELA and DAS and compared to actual remaining days on orbit based on the TLEs. At the initial decay time (day 0) the actual TLE data of the Castor satellite yields orbital decay in 383 days. Simulations with the "day 0" TLE were run in STELA and DAS and yielded an estimation of decay in 322 days and 338 days, respectively. Each subsequent plot on the graph represents other iterations from STELA and DAS, using the corresponding TLEs. Both estimators initially underestimate the decay time, then gradually match with the actual decay about 100 days prior to reentry, and slightly overestimate near the end of the decay. It is clear in these examples that a longer decay time will yield a greater underestimation.

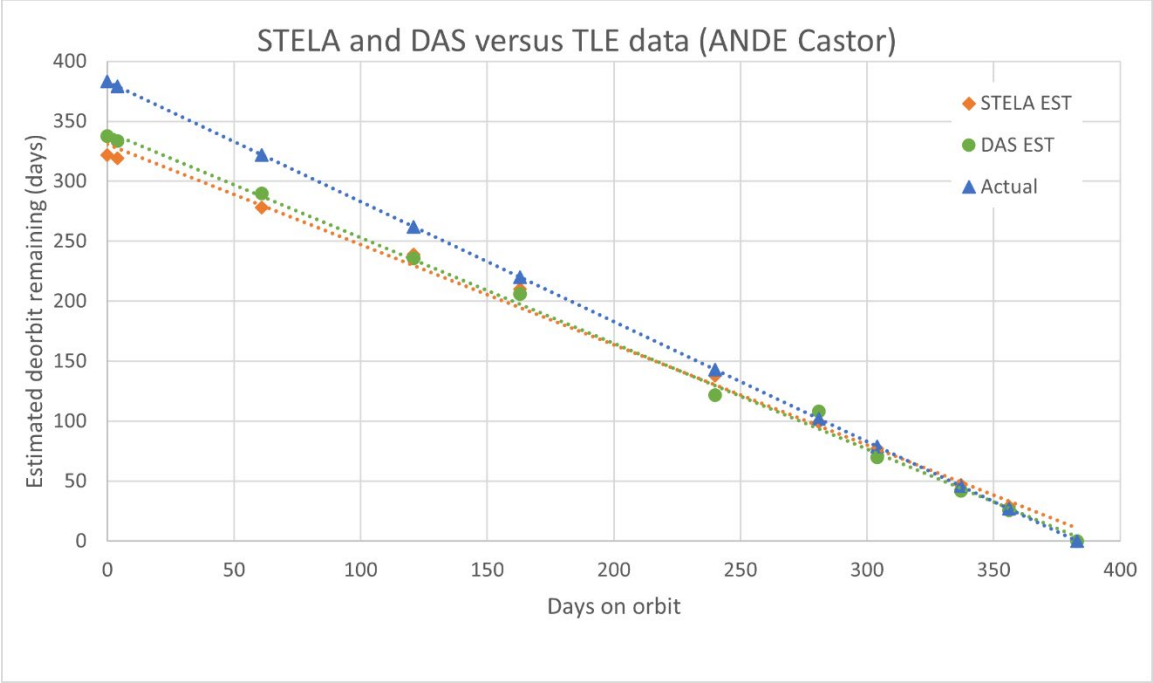

Figure 4. Actual vs. predicted de-orbit time for ANDE Castor using STELA and DAS estimates.

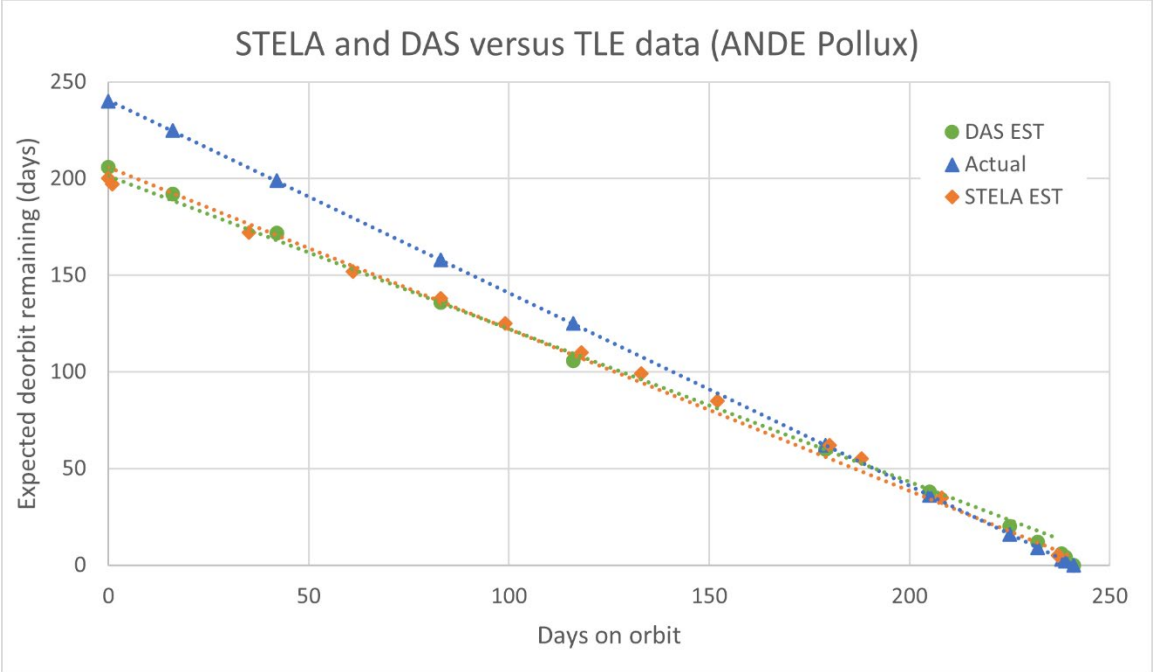

Figure 5. Actual vs. predicted de-orbit time for ANDE Pollux using STELA and DAS estimates.

THIS PAGE INTENTIONALLY LEFT BLANK

III. MODELING AND CASE STUDIES FOR SPACECRAFT ORBITAL DECAY

A. DATA SOURCES AND MODELING APPROACH

Modeling is accomplished in three phases. The first phase takes the known information of a satellite and estimates the decay in STELA using currently available satellite specifications (i.e., mass, surface area or dimensions). Actual or expected EOL or deactivation date, if applicable, is also used to determine the orbital regime wherein the satellite begins or continues its decay. TLE data from SpaceTrack.org provides the actual orbital parameters from the expected EOL. Phase one provides the baseline decay time to compare to the benefits of including a drag device. If the satellite de-orbits within 25 years, no further analysis is required, although the intent is to identify satellites that do not fall into this category. Phase two uses STELA to estimate the necessary increase in surface area required to de-orbit the spacecraft within 25 years. Initial phase two results are presented. However, some cases require an increase in surface area that may be unrealistic. Phase three addresses these scenarios by including a hybrid propulsion-drag de-orbit scheme for optimal mass-savings.

B. EFFECTIVE CROSS-SECTIONAL AREA DETERMINATION

A significant uncertainty in the estimations is determining the effective cross-sectional area for each satellite in calculating the ballistic coefficient via Equation 1. Spacecraft under active control typically project a singular cross-sectional area towards the direction of flight (this is the area over which the drag force acts). Defunct or passivated spacecraft may tumble, spin, or settle into "preferred" attitudes based on drag forces or even collisions with other debris. For simplicity and consistency in comparison with other spacecraft, it was assumed that all spacecraft are tumbling.[4] A tumbling satellite has an equal likelihood of projecting a surface to the drag force, thus this area is estimated as the total surface area of spacecraft divided by four. For convex shapes, this formula provides an estimate of the average cross-sectional area for a tumbling object [16]. For the satellites

[4] This is consistent with other broad studies of spacecraft decay [1], [2].

examined in this study, the effective cross-sectional areas that were determined by the source are used if possible. However, most cross-sectional areas are derived from the available geometry of the satellite's specifications. Likewise, when determining the necessary increase of effective cross-sectional area that would be provided by the drag device, the same technique is used. This means that the increase in effective cross-sectional area equals the total surface area of the drag device divided by four. While it is recognized that the addition of a drag device would further tend to favor a "preferred" orientation during decay, the orientation cannot be predicted without detailed analyses. For this reason, and for consistency with prior studies, the "one-quarter tumbling rule" is retained herein.

Table 2 contains a set of satellites that were examined. Referring to the DMSP 5D-2 spacecraft example, the geometric dimensions of the bus are found in [17]. The description states that the bus is a 6.7 m long cylinder, radius 0.75 m, and that the solar array is rectangular with specified surface area of 9.2 m^2. Therefore, the estimation of total surface area is simply the surface area of the bus plus the surface area of the solar array.[5] In this case, the surface area of the cylinder is given by the equation below, where r = radius and h = height [16].

$$SA_{Cylinder} = 2\pi \cdot rh + 2\pi \cdot r^2 = 35.1\ m^2$$

$$SA_{SolarArray} = 2 \cdot 9.2\ m^2 = 18.4\ m^2$$

$$Effective\ CrossSectional\ Area = \frac{(35.1\ m^2 + 18.4\ m^2)}{4} = 13.4\ m^2 \qquad (2)$$

This same approach applies to the other satellites in this study, based on the geometric description of the satellite bus, payload, and solar panels (see Appendix A for estimates and calculations for each satellite studied). If given, such as EO-1 from a report from NASA [7], the reported effective cross-sectional area was used instead.

[5] Smaller appendages such as the solar array attachments are neglected for simplicity. This has the added benefit of adding a bit of conservatism by underestimating area.

C. CASE STUDY AND MODELING TECHNIQUE VALIDATION

The first group of satellites examined were the Defense Meteorological Space Program (DMSP) Block 5D series. These offer a useful example of a group of satellites that remain on orbit well after their EOL. Of the 10 satellites examined below, all of them continue to orbit today, and while launched prior to regulation, Table 2 shows many are predicted to remain on orbit into the next century. For example, using STELA, the shortest de-orbit time, from natural decay alone, exceeds 94 years after its EOL. Table 2 summarizes the 10 inactive DMSP satellites and their respective modeled decay times.

Table 2. Inactive DMSP satellites with estimated de-orbit times from natural decay. Adapted from [17].

Satellite	EOL Year	Projected De-orbit Year	Estimated Total Years to De-orbit
DMSP 5D-1 (F-3)	1979	2077	98
DMSP 5D-2 (F-6)	1987	2107	120
F-7	1987	2106	119
F-8	1991	2141	153
F-9	1988	2109	121
F-10	1995	2089	94
F-11	2000	2184	184
F-12	1994	2178	184
F-13	1995	2141	146
F-14	1997	2141	144

As displayed above, none of these spacecrafts would have been compliant with the 25-year debris mitigation regulation. However, the analysis above includes assumptions and is only a result of simulations, not reality. Much like the validation case studies, the historic SpaceTrack.org TLEs can be used to help better understand the reality of each orbit. DMSP 5D-1 (F-3), for example, reached its EOL in 1979. It is safe to assume at this point that there would be no further orbit raising maneuvers and that the spacecraft is tumbling. If the solar activity over that period matches the model in STELA, and if the estimates of the effective cross-sectional area and mass are accurate, then the modeling in STELA from a TLE in 1979 should yield a result similar to the most recent TLE

parameters. This confirmation step is different from the validation case studies earlier because there is added uncertainty associated with the cross-sectional area estimation and this includes effects of at least two complete solar cycles, rather than less than a year. Here, if the area estimation is too large (or similarly the mass too small), then the simulation will show more decay than reality. Table 3 compares the modeling after 41 years through STELA to the actual orbit parameters taken from a recent TLE from SpaceTrack.org. The result is consistent with the validation case studies, meaning that the satellite did not decay as much in reality as the simulation with respect to perigee, but the difference was not significant enough to indicate that there is additional error with respect to the area estimation.

Table 3. DMSP 5D-1 (F-3) comparing STELA simulation (with 1979 TLE) to 2020 TLE. Adapted from [4], [17].

Parameters	**TLE Actual (1979)**	**TLE Actual (2020)**	**STELA Modeled to 2020**	**Delta**
Date (y-m-d)	1979-05-01	2020-05-01	2020-05-01	41 yrs
Z_p (km)	815	764	744	20 km
Z_a (km)	826	778	784	-6 km

To understand this further, it is important to determine how much a 20 km difference after 41 years will affect the overall decay time. For example, a relatively small deviation early in the decay due to higher-than-average solar activity or other sources could create a large difference once viewed with respect to the total years to de-orbit. Table 4 takes the results of a simulation when using a TLE from 1979 and compares it to a simulation that begins from an updated TLE from 2020. For this example, the variation only creates a difference of approximately one year of total de-orbit time.

Table 4. DMSP 5D-1 (F-3) comparing two separate TLEs for de-orbit time

Parameters	Using 2020 TLE	Using 1979 TLE
Projected De-orbit Date (y-m-d)	2077-03-17	2075-12-07
De-orbit Duration	~98 years	~97 years

The results suggest that the calculated cross-sectional area estimate is adequate for the purposes of this study. Additionally, recent TLEs for all satellites modeled were used to improve accuracy. This was done to remove the associated error in modeling for longer propagation times. The satellites examined in this study used TLEs from 1 Feb 21 and later.

THIS PAGE INTENTIONALLY LEFT BLANK

IV. DE-ORBIT ANALYSES

The de-orbit analyses consist of data from 11 satellites.[6] These spacecrafts were selected based primarily on ballistic coefficient and orbital altitude, targeting the "pink" area of Figure 1 (Region 2). Data availability and geometric simplicity also played a role in selecting these satellites. The satellite specifications were collected from [7], [17]–[23] and the TLE date from [4]. The analysis in this section first summarizes these midsized satellites, shown in Table 5. Simulations in STELA determined the necessary ballistic coefficient required to decay each spacecraft within 25 years along with the associated area of a notional drag device. Next, each scenario was examined to determine a practical de-orbited method. The two methods, identified in Table 6, included either the use of a drag device alone, or a propulsion burn in combination with a drag device. Finally, the analyses determined possible mass savings for each scenario, which provides insight into the practicality and usefulness of employing a drag device. Of the 11 satellites discussed in this section, 10 of them were demonstrated to be practical with respect to the criteria outlined in this section.

[6] Figure 6 includes plots for 12 satellites; however, Ikonos-2 is included to show a data point that will de-orbit within 25 years without a drag device or propulsion. This data point shows where a spacecraft will decay naturally based on its altitude and ballistic coefficient. Ikonos-2 is not analyzed further with respect to drag device enhancement; i.e., fuel mass savings or decreased de-orbit time.

Table 5. Summary of midsized satellites data used in this study.

NORAD ID	Name	Mass (kg)	Zp (km)	Effective Cross-sectional area (m^2)	Current De-orbit Lifetime (years)	C_B Original	C_B Required	Required Drag Device Area (m^2)
29108	CALIPSO	635	681	10.0	27.5	31.6	28.9	1.9
29107	CloudSat	995	682	12.3	36.9	40.5	27.6	11.4
26619	EO-1	548	671	6.0	38.0	45.4	22.5	12.3
40059	OCO-2	449	699	3.0	90.2	74.1	22.5	13.9
10820	F-3	513	763	13.4	53.7	19.2	9.9	25.2
25758	IRS-P4	1050	719	18.5	46.2	28.4	14.6	35.0
31113	HY-1B	442	778	7.6	99.9	29.0	7.9	40.7
13736	F-6	750	786	13.4	100.0	28.0	6.9	81.2
14506	F-7	750	787	13.4	101.0	28.0	6.8	83.2
21798	F-11	830	824	13.4	178.0	31.0	4.2	169.2
19467	FY-1A	750	870	9.3	369.0	40.5	2.9	241.4

Data drawn from [4], [7], [17], [18], [19], [20], [21], [22], [23]. This table lists the midsized satellites specifications, perigee altitude obtained from recent TLEs [4], and calculated effective cross-sectional area. STELA was used to determine the current de-orbit lifetime and subsequently the "25-year" de-orbit lifetime with an adjusted cross-sectional area input and ballistic coefficient (C_B) required.

A. MIDSIZED SATELLITES AND CASE STUDY SUMMARY

Figure 6 is a plot of the data in Table 5 for 11 different satellites, each having three data points. Each satellite has a unique associated initial altitude (*Zp*, plotted on the x-axis), so the three data points for each satellite are aligned in a column. The blue diamond represents the satellite's original ballistic coefficient (left y-axis). The orange square represents the required ballistic coefficient necessary to de-orbit within 25 years. The original and required ballistic coefficients are paired in an outlined box. The yellow triangle represents the area increase (right y-axis) that would be necessary to achieve the required ballistic coefficient. For example, IRS-P4 has an original ballistic coefficient of approximately 28 kg/m^2, a required ballistic coefficient of approximately 19 kg/m^2 to meet the 25-year de-orbit boundary, and a resulting drag area increase of 35 square meters.

Both the altitude and the satellite's mass play a factor in determining the necessary area increase. Therefore, the plot below shows a variety of ballistic coefficient deltas and associated drag device dimensions necessary to de-orbit within 25 years. For example,

OCO-2 requires a ballistic coefficient decrease of nearly 52 kg/m^2 to achieve a de-orbit within 25 years yet would only require a 13.9 square meter drag device area. Conversely, DMSP (F-11) requires a 169 square meter drag device, despite only needing a decrease of BC of 27 kg/m^2. The relatively large area increase for F-11 is due to the significantly higher altitude and mass when compared to OCO-2.

It was previously noted that spacecraft above approximately 850 km orbits are not good candidates for drag enhancement due to the variabilities and uncertainties from solar radiation pressure above that altitude. The right side of Figure 6 further illustrates the impracticality of drag enhancement in this regime—very large areas of drag enhancement are necessary to sufficiently lower the altitude for F-11 and FY-1A, even while ignoring SRP. While the IKARUS solar sail spacecraft [24] has deployed such a large area, the sail also utilized much of the spacecraft mass and area as the primary mission. Alternatives for the F-11 and FY-1A satellites would be the combination of a reasonably sized drag device with a shorter propulsive burn—analyzed and discussed in later.

Note that unlike Figure 1, the ballistic coefficient is not plotted on a logarithmic scale in Figure 6. Here the region of interest (Area 2 of Figure 1) is examined in more detail. The estimated 25-year boundary appears here as an exponential line as a result (orange dotted line). The necessary area increase has a linear relationship with C_B (see Equation 1), so it is plotted in a linear curve fit (grey dotted line).

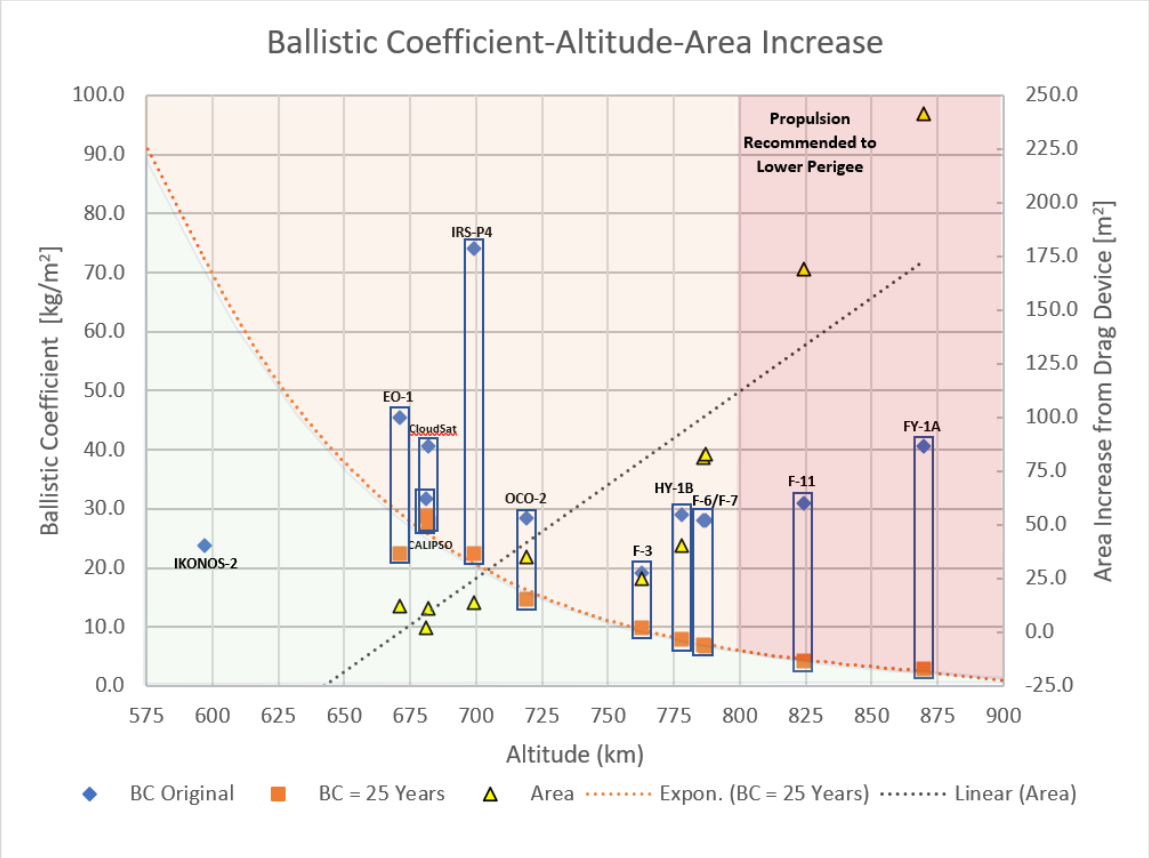

Data drawn from [4], [7], [17], [18], [19], [20], [21], [22], [23]. The original ballistic coefficient (blue diamond) is compared to the necessary ballistic coefficient (orange square) to decay within 25 years. The area increase (yellow triangle) that would be produced from a drag device, varies for each case. The shaded green area represents the ballistic coefficient region where spacecraft will decay in less than 25 years and the orange region more than 25 years. The red shaded area is where it is recommended to use propulsion to initially lower perigee because the drag device area becomes excessive (above 800 km) and above solar radiation pressure (above 850 km) becomes the dominant force.

Figure 6. Ballistic coefficient and drag area increase necessary for the set of midsized satellites.

B. DE-ORBIT METHODS

As the ballistic coefficient and orbital altitudes vary, so do the strategies for de-orbit. This study examines the following two scenarios: first, the spacecraft can be successfully de-orbited within 25 years simply by deploying a drag device in lieu of propulsion; second, the spacecraft will use some propulsion to initially lower perigee and then deploy a drag device to de-orbit within 25 years.

To determine which satellites in our study dataset can be de-orbited with a drag sail alone, a practical area for a drag device should be defined. A practical value depends on design drivers discussed in Chapter I—the drag device must stow in a compact container, and the device must be low mass (relative to fuel displaced), very simple to operate and reliable enough to perform for the first time at the end of mission. Reviewing the summary data in Rhatigan and Lan [3], Table 1, the largest drag device area they identified for the small satellites flown successfully to date is 14 m^2 (dragNET^{TM}) [25]. Midsized satellites can presumably accommodate larger devices and have more surface area for modular accommodation of multiple devices (see, for example, the modular design in [2]). An area 2.5 times this value was selected, 35 m^2, based on this rationale. Table 6 indicates by shading which of the spacecraft in our data set could self-dispose by addition of a drag area of 35 m^2 or less.

Table 6. Summary of midsized satellites with required area increase for de-orbit.

NORAD ID	Name	Mass (kg)	Zp (km)	Effective Cross-sectional area (m^2)	Current De-orbit Lifetime (years)	C_B Original	C_B Required	Required Drag Device Area (m^2)
29108	CALIPSO	635	681	10.0	27.5	31.6	28.9	1.9
29107	CloudSat	995	682	12.3	36.9	40.5	27.6	11.4
26619	EO-1	548	671	6.0	38.0	45.4	22.5	12.3
40059	OCO-2	449	699	3.0	90.2	74.1	22.5	13.9
10820	F-3	513	763	13.4	53.7	19.2	9.9	25.2
25758	IRS-P4	1050	719	18.5	46.2	28.4	14.6	35.0
31113	HY-1B	442	778	7.6	99.9	29.0	7.9	40.7
13736	F-6	750	786	13.4	100.0	28.0	6.9	81.2
14506	F-7	750	787	13.4	101.0	28.0	6.8	83.2
21798	F-11	830	824	13.4	178.0	31.0	4.2	169.2
19467	FY-1A	750	870	9.3	369.0	40.5	2.9	241.4

Adapted from [4], [7], [17], [18], [19], [20], [21], [22], [23].This table contains the same data as Table 5 but identifies which satellites could de-orbit within 25 years using a 35 m^2 drag device. Propulsion or a combination of drag and propulsion would be required (highlighted grey) for satellites that would not decay within 25 years from the inclusion of a 35 m^2 drag device alone.

Referencing Table 6, some interesting trade-offs for the satellites in higher orbits become apparent. Satellite F-11 is a clear example of an impractical satellite to de-orbit with the use of a drag device alone since it requires an area of over 150 m^2. However, utilizing a drag device in combination with an orbit-lowering propulsive maneuver may prove useful due to potential mass savings. CALIPSO requires a drag device that is 1.9 m^2. While this is well-proven as a practical area to achieve, the higher orbit creates a conundrum with respect to mass trade-offs (explored later in this section). Additionally, CALIPSO is a poor candidate for "significantly" reducing its area-time product as the small decrease in de-orbit time yields ~6 (m^2·year) decrease. OCO-2, IRS-P4, and F-3 are examples of satellites that initially appear to be practical for application of a drag device. This is because the area increase is achievable (less than 35 m^2) and the de-orbit lifetimes are significantly reduced from an excess of 45 years or more. Validation of these candidates, as well as the candidates that require propulsion, are discussed further with respect to fuel mass savings.

The two approaches to de-orbit in LEO include lowering perigee to approximately 75 km (for an immediate de-orbit) or to an altitude where the satellite will decay naturally within a specified time [8]. This analysis uses STELA to determine the maximum perigee altitude that would facilitate a 25-year decay for F-6, F-7, F-11, FY-1A, and HY-1B. Using F-11 in a "what-if" example, there are two steps to the required de-orbit. First, a propulsive maneuver lowers the orbit so that the 25-year decay can be achieved. Second, the orbital decay of the satellite is seen in Figure 7 starting with a perigee of 566 km. (Also note the solar cycle effects modeled within STELA, particularly where the apogee decreases more rapidly around years 4, 14 and 23.)

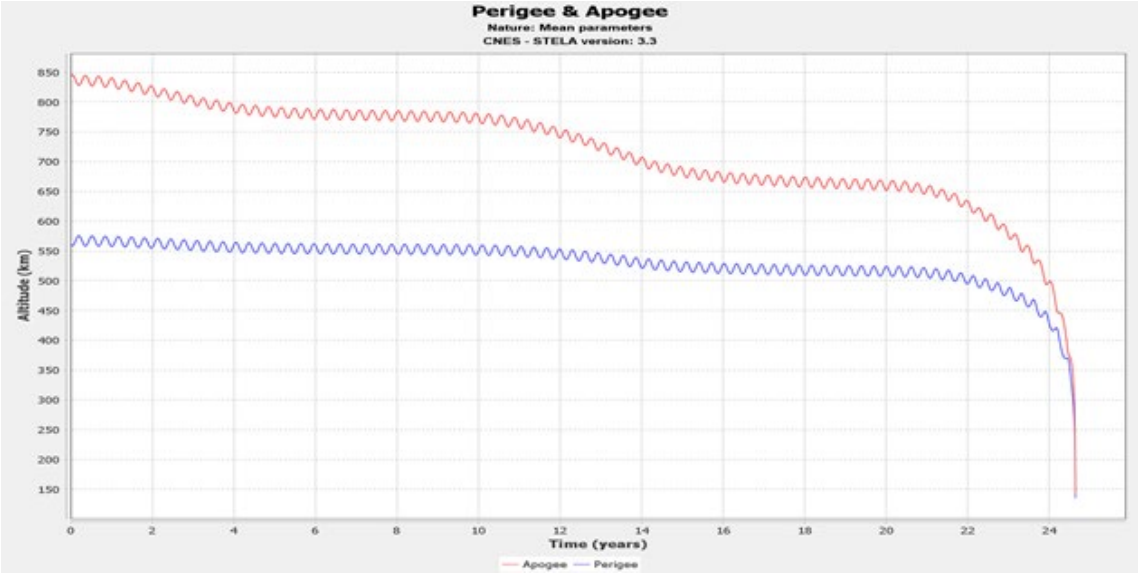

Figure 7. Satellite F-11 decay after perigee lowering propulsion maneuver.

After determining a perigee altitude that would successfully de-orbit the satellite within 25 years without a drag device, the ΔV necessary to lower perigee via propulsion was calculated to be 68 m/s. The calculations for this step are shown in equations below from [8], and the variables and constants are defined in Table 7.

Table 7. Propulsion calculation list of variables and constants.

Symbol	Definition
a	Semi-major axis
e	Eccentricity
v_a	Velocity at apogee
v_p	Velocity at perigee
μ	Earth gravitational constant
r_a	Radius of apogee
r_p	Radius of perigee

$$v_a = \sqrt{\frac{\mu(1-e)}{a(1+e)}};\ e = \frac{r_a - r_p}{r_a + r_p}\ ;\ a = \frac{(r_a + r_p)}{2}$$

$$r_a = 6378\ km + 843\ km = 7221\ km$$

$$r_{p(inital)} = 6378\ km + 824\ km = 7202\ km$$

$$a_{initial} = \frac{(7221\ km + 7202\ km)}{2} = 7211.5\ km$$

$$e_{initial} = \frac{7221\ km - 7202\ km}{7221\ km + 7202\ km} = 0.00132$$

$$v_{a(intial)} = \sqrt{\frac{398600\frac{km^3}{s^2} \cdot (1 - 0.00132)}{7211.5\ km \cdot (1 + 0.00132)}} = 7.425\ km/s$$

$$r_{p(deorbit)} = 6378\ km + 566\ km = 6944\ km$$

$$e_{deorbit} = \frac{7221\ km - 6944\ km}{7221\ km + 6944\ km} = 0.0196$$

$$v_{a(deorbit)} = \sqrt{\frac{398600\frac{km^3}{s^2} \cdot (1-0.0195)}{7082.5\ km \cdot (1+0.0195)}} = 7.357\ km/s$$

$$\Delta v = 7425\ m/s - 7357\ \text{m/s} = 68\ \text{m/s}$$

Similarly, DAS was used to validate the ΔV necessary for the satellites based on their area-to-mass ratio in Figure 8. F-11, with an area-to-mass ratio of ~0.016 m^2/kg (blue), with an initial apogee altitude of 843 km, aligns with the calculated 68 m/s. These values are also tabulated in Table 8, in the column labeled "Required ΔV without Drag Device (m/s)." This column represents the fuel "baseline" for comparison to determine if a drag device can produce savings over the conventional propulsive de-orbit procedure.

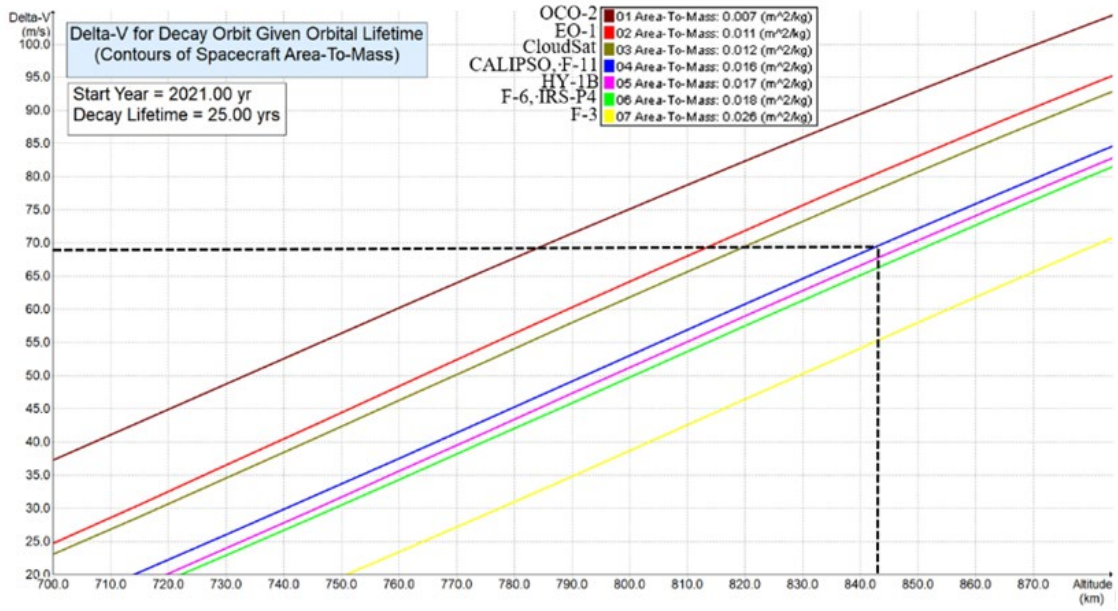

Figure 8. Delta-V required for 25-year decay based on altitude and area-to-mass ratio.

After determining the change in velocity to lower the orbit to a perigee that facilitates a 25-year decay, the process was repeated for the inclusion of a drag device. The results appear in Table 8, in the column labeled "Required ΔV with Drag Device (m/s)," and the calculation is explained in the following Section C. This analysis assumed a 35 m^2 area increase from a drag device (previously discussed as a maximum reasonable value). STELA was used to determine a new perigee altitude that would decay the F-11 satellite, but with the increased effective cross-sectional area that would come from the introduction of a drag device. For F-11, for example, the perigee would only need to be lowered to an altitude of 624 km, vice 566 km, if a 35 m^2 drag device was used. Likewise, this sized drag device would result in a decrease of ΔV, reducing the requirement from 68 m/s to 53 m/s. In the following section, this is translated into fuel mass savings.

C. MASS TRADE-OFF

Given that drag devices can displace de-orbiting fuel and, in some cases, entire propulsion systems, one question driving the adoption of drag devices for this purpose is

what are the mass trade-offs if a spacecraft developer chooses to adopt this technology? Designers may also elect to extend a mission with that fuel budget and add the mass of a drag device to the spacecraft for self-disposal. Either way, mass trade-offs are necessary to optimize design.

Of the spacecraft examined in Table 7, five of them would require a perigee lowering maneuver to de-orbit within 25 years, assuming that a practical drag device is no larger than 35 m^2. For the F-11 example, it is shown above that the perigee lowering maneuver with a drag device would use less ΔV, which directly relates to less fuel and less mass. To calculate an estimation of the potential mass savings, the five satellites (F-6, F-7, F-11, HY-1B, and FY-1A) assumed a 35 m^2 drag device would be deployed after a perigee lowering maneuver. The ΔV for the higher perigee was then calculated for each case (as shown above for F-11). Next, each satellite's mass requirements were estimated from the rocket equation, Equation 3. Since every satellite may have a unique engine, a consistent propulsion system was used to compare the different cases. Each case assumed a hydrazine, monopropellant propulsion system with an exhaust velocity (v_e) of 2100 m/s. This assumption is based on a typical monopropellant specific impulse (I_{sp}) range of 200–235 seconds [8], which yields a v_e from the relationship below [8]:

$$v_e = I_{sp} \cdot g_0 \tag{3}$$

$$215\,\text{sec} * 9.81\frac{m}{s^2} \cong 2100\,m/s$$

Using the simplified rocket equation below, the initial mass (m_o) is calculated to determine the mass required for the perigee lowering maneuver. For this calculation, the spacecraft dry mass is assumed to be the final mass (m_f), which varies for each satellite. Equation 4 [8] shows the calculation used to determine the mass requirement for F-11:

$$\boldsymbol{\Delta v = v_e\, ln\left(\frac{m_0}{m_f}\right) \Rightarrow m_f \cdot e^{\Delta V/v_e} = m_o} \tag{4}$$

For F-11, m_f = 830 kg; ΔV = 53.6 m/s (with drag device) and ΔV = 68 m/s (with no drag device).

$$\boldsymbol{m_0\ (without\ drag\ device) = 830\ kg \cdot 2.71^{\frac{68.1\frac{m}{s}}{2100\frac{m}{s}}} = 857.4\ k}$$

$$\boldsymbol{m_0\ (with\ drag\ device) = 830\ kg \cdot 2.71^{\frac{53.6\frac{m}{s}}{2100\frac{m}{s}}} = 851.4\ k}$$

For F-11, approximately 6 kg of fuel could be saved if a drag device had been utilized in combination with a de-orbiting maneuver. Since the perigee altitude requirement is higher when using a drag device, there is less fuel and therefore less mass needed to accomplish this. Of note, more efficient propulsion systems (higher v_e) would reduce the impact of a drag device with respect to mass savings. Additionally, the mass of the drag device itself has not been included here, but certainly would play a factor in determining the practicality of its employment. For example, if the fuel mass required to lower perigee is less than the drag device, the inclusion of a drag device would be difficult to justify on a mass trade-off alone. As noted earlier, this "displaced" fuel could also be used to extend mission or meet other mission requirements, so the trade-off is very design and mission specific. Another notable advantage for satellites at higher orbits: an initial propulsive maneuver lowers the satellite into the altitude range where drag devices are most effective. The analysis is summarized in Table 8.

For the spacecraft in this study that would de-orbit with a drag device alone, it can be assumed that the drag device completely replaces the fuel mass requirement that would have been needed for a perigee lowering maneuver. Table 8 shows the potential mass savings for the satellites examined. Savings available range from 1.5 kg to 10 kg of offset fuel. The perigee altitudes that would have been necessary to de-orbit within 25 years are used to determine how much mass would have been saved if a drag device were to be employed. For the spacecraft that would require propulsion regardless, the difference in ΔV is used to determine the mass savings.

Table 8. Potential fuel savings for a set of midsized satellites.

NORAD ID	Name	Mass (kg)	Zp (km)	Perigee Altitude to Decay < 25 Years (km)	Required ΔV without Drag Device (m/s)	Required ΔV with Drag Device (m/s)	Fuel Mass Savings with Drag Device (kg)
29108	CALIPSO	635	681	665	5.1	0	1.5
29107	CloudSat	995	682	625	15.2	0	7.2
26619	EO-1	548	671	609	16.6	0	4.3
40059	OCO-2	449	699	535	44.1	0	9.5
10820	F-3	513	763	664	26.1	0	6.4
25758	IRS-P4	1050	719	644	19.9	0	10.0
31113	HY-1B	442	778	592	49.3	23.7	5.5
13736	F-6	750	786	590	52.2	33.4	6.9
14506	F-7	750	787	590	52.2	35.6	6.1
21798	F-11	830	824	560	68.2	53.6	5.9
19467	FY-1A	750	870	520	92.3	72.1	7.5

V. DRAG DEVICE DESIGN

A. ESTIMATE OF MASS REQUIREMENTS

The potential for mass savings based on the satellites analyzed range from 1.5 kg to 10 kg; however, this did not consider the additional mass of the drag enhancing device itself. Given the function of the device, clearly it is desirable to make a drag enhancing device with the least amount of mass possible. Current devices exist that are less than 0.5 kg [26] for a CubeSat. While "sail" materials are very lightweight, the mass of a drag device is expected to scale with the area needed. The IKAROS solar sail, for example, provided an area of 196 m^2 and had a mass of approximately 14 kg [24]. While this was considered too large and impractical for this study, a drag device the size of IKAROS would have been able to self-dispose all the satellites in this study apart from FY-1A. However, even FY-1A could de-orbit within 25 years, from a drag device alone, if the area increase were large enough (~241 m^2) and the effects from SRP were neglected. As demonstrated earlier (Figure 6), when the altitude increases, the drag device area will increase linearly to the point where the mass of the device may be greater than the fuel necessary to lower perigee.

To explore this trade-off, rough estimates of drag device masses were scaled from a known device for a range of midsized satellites (600–1000 kg). These estimates were then plotted against altitude to determine expected practical limits of altitude as seen in the previous section. This was estimated in STELA by simulating these notional satellites at various altitudes with correspondingly sized drag devices. The device mass was estimated by scaling sail density to that of the IKAROS solar sail. A 15% margin was included over IKAROS [24]. Assuming a direct relationship of area to mass, IKAROS produces 14 m^2 for each 1 kg of material. A more conservative ratio of 11.9 m^2 per kilogram of material was applied to the notional satellites below. These estimates use the same assumptions with respect to propulsion performance as in Chapter IV. A more efficient propulsion system would reduce the mass savings offered by a drag device. Also note that for some satellites, the entire propulsion system could be eliminated, as it is only used for de-orbit. That analysis is beyond the scope of this study so is not addressed.

Figures 9, 10 and 11 illustrate the trade-off boundary. It occurs in the range of 850–900 km, for a 1000 kg, 800 kg, and 600 kg satellite mass, respectively. Above this trade-off boundary altitude, the mass savings from a drag device becomes negative (that is, the drag device would weigh more than the fuel saved), though altitudes above 850 km have been previously excluded because of the dominance of SRP. Indeed, using these gross assumptions, mass savings may be realized for all cases below the SRP "boundary" of approximately 850 km (see Figure 1).

The more massive satellite (1000 kg, Figure 9) can achieve more mass savings than the 800 kg (Figure 10) and 600 kg (Figure 11) satellites. Not only is the difference from fuel mass to device mass larger, but the altitude at which the device is effective is slightly higher. For example, in Figure 9, the cross-over point exceeds the SRP boundary at approximately 900 km. For the 600 kg satellite, the cross-over occurs at an altitude of ~875 km. Similarly, the greatest potential mass savings for the 1000 kg satellite is ~8.6 kg. Correspondingly, the smaller satellite may realize smaller savings; the 600 kg satellite may realize at most ~3.3 kg.

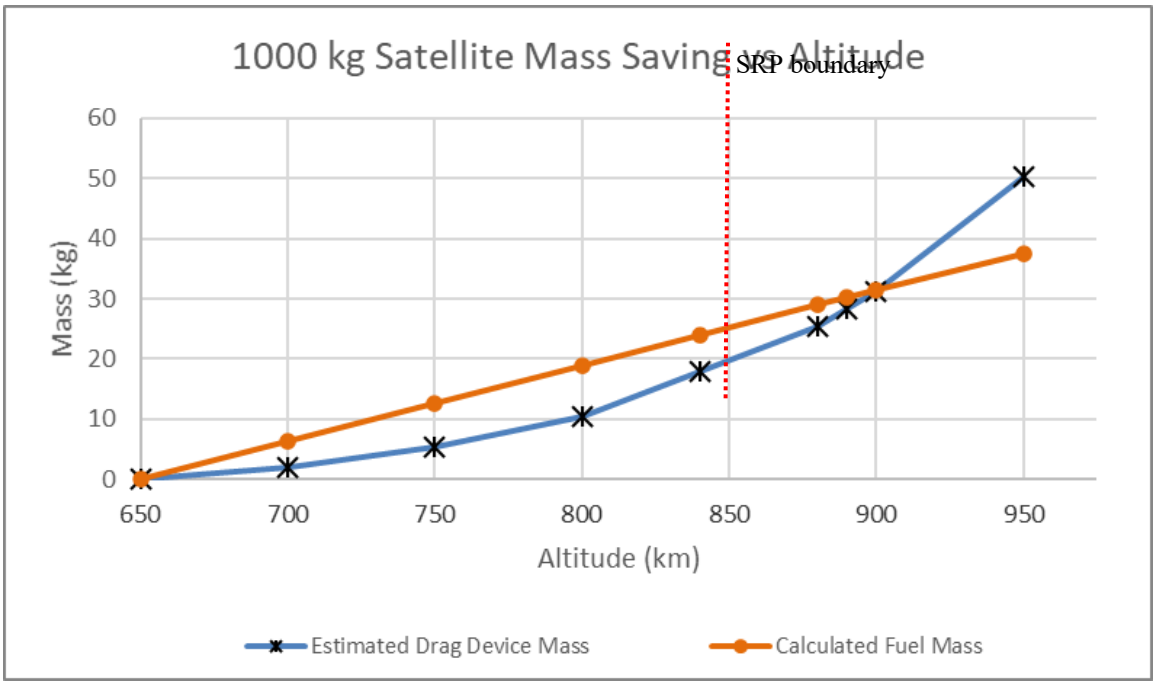

Figure 9. Potential mass trade-off vs. altitude for de-orbit of a notional 1000 kg satellite

This graph shows the difference in mass of a notional 1000 kg satellite for various altitudes. The calculated fuel mass is what would be needed to lower perigee to an altitude to decay naturally within 25 years, while the estimated drag device mass is what would decay it without propulsion based on practical drag device estimates. The difference between the two represents the best possible mass savings. Note that above ~900 km, the drag device mass is more than the fuel. The largest possible savings is ~800 km and could save ~8.5 kg of mass.

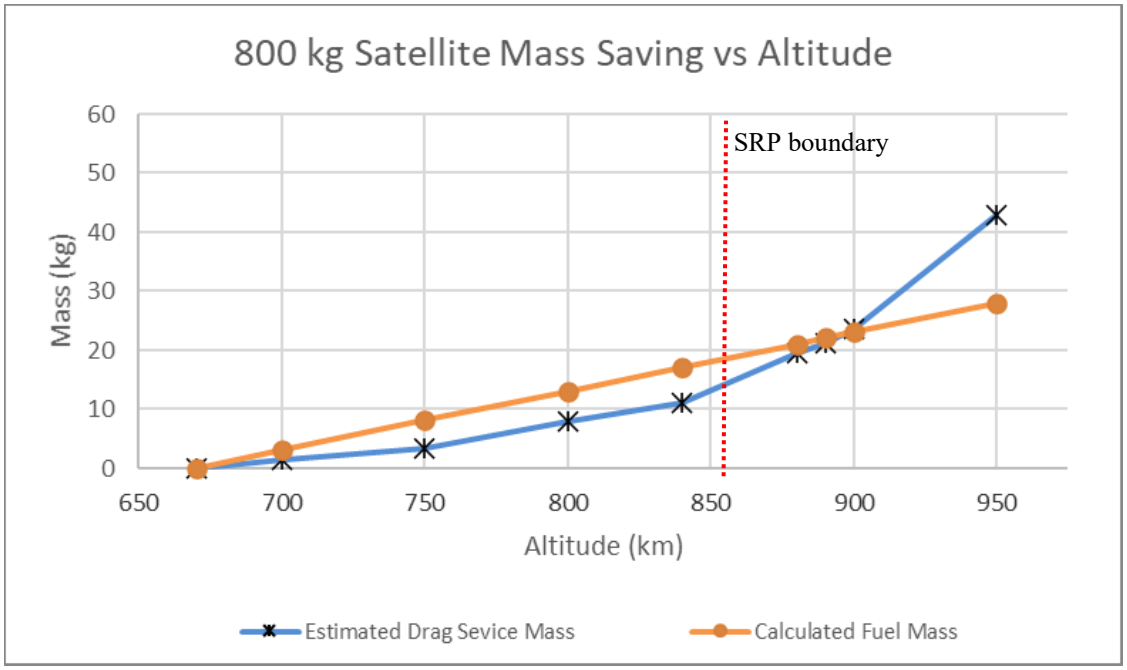

Figure 10. 800 kg satellite mass savings vs. altitude

This graph shows the difference in mass of a generic 800 kg satellite for various altitudes. Note that above ~880 km, the drag device mass is more than the fuel. The largest possible savings is ~840 km and could save ~5.9 kg of mass.

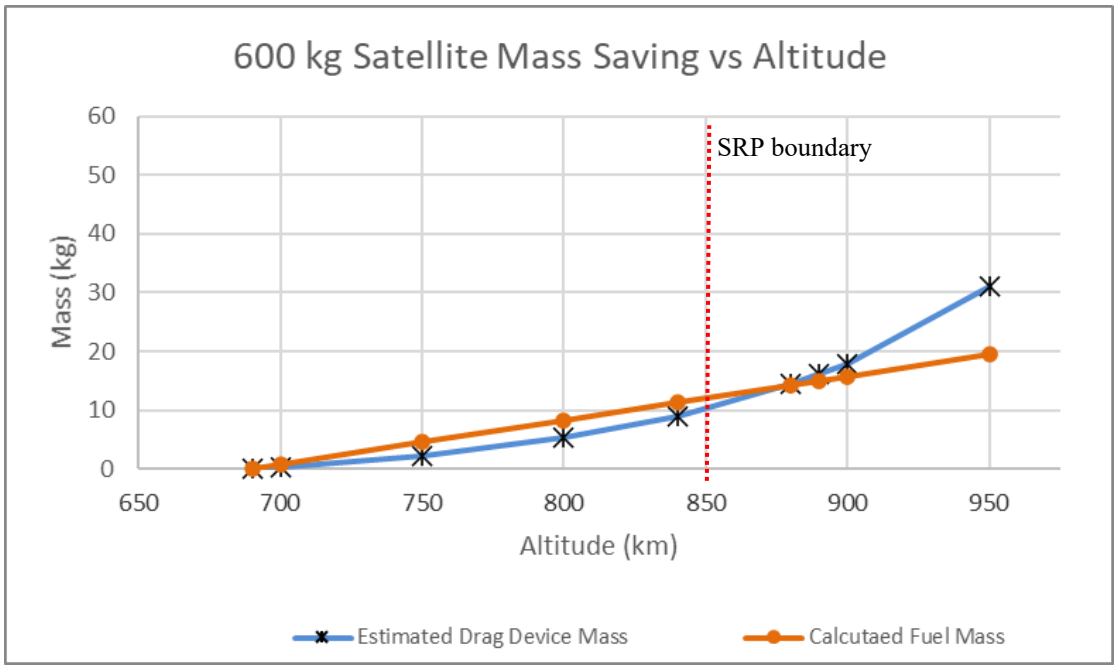

Figure 11. 600 kg satellite mass savings vs. altitude

This graph shows the difference in mass of a generic 600 kg satellite for various altitudes. Note that above ~875 km, the drag device mass is more than the fuel. The largest possible savings is ~800 km and could save ~3.3 kg of mass.

As noted earlier, there is a practical limit to how large a drag device can be, estimated at 35 m^2. Of course, mass is not the only design consideration; as noted in the summary of design requirements in Chapter I, section C, complexity, reliability, and non-interference with the primary mission also need to be addressed. From Table 9, fuel mass savings for satellites require a propulsive maneuver ranging from 5.5 kg to 7.5 kg. Figures 9–11 show rough estimates of device mass in the range of 5 to 15 kg. Therefore, a good design goal for the mass of a 35 m^2 drag device might be 5 kg.

Further, if a scalable device could be implemented, it would provide flexibility and limit unnecessary mass to a spacecraft. Table 10 shows the fuel mass savings when the drag device mass is included for both a fixed 35 m^2 device and a scalable device. It assumes a 5 kg, 35 m^2 device and deducts the "excess mass" by using the same ratio of 11.9 m^2 for each 1 kg of material, used earlier.

Table 9. Potential fuel savings with mass of a scalable device included.

NORAD ID	Name	Area of Drag Device for Decay	Fuel Mass Savings with Mass-less Drag Device (kg)	Fuel Mass Savings with 5 kg Drag Device (kg)	Fuel Mass Savings with Scalable Drag Device (kg)
29108	CALIPSO	1.9	1.5	-3.5	-0.7
29107	CloudSat	11.4	7.2	2.2	4.2
26619	EO-1	12.3	4.3	-0.7	1.2
40059	OCO-2	13.9	9.5	4.5	6.3
10820	F-3	25.2	6.4	1.4	2.2
25758	IRS-P4	35.0	10.0	5.0	5.0
31113	HY-1B	40.7	5.5	0.5	0.5
13736	F-6	35.0	6.9	1.9	1.9
14506	F-7	35.0	6.1	1.1	1.1
21798	F-11	35.0	5.9	1.6	1.6
19467	FY-1A	35.0	7.5	2.5	2.5

Table 9 highlights reasonable design requirements for a drag enhancing device. If the device is more than 5 kg to provide 35 m^2 of area, it begins to cost more in mass than a traditional propulsion burn. A scalable device adds increased fuel mass savings.

B. PROTOTYPES AND REQUIREMENT REFINEMENT

While the IKAROS solar sail provided insight on the scope of possible mass-related trade-offs, other drag devices will likely have a higher mass to area ratio. Prototypes such as the drag device in [27] are designed to produce approximately 6 m^2 of effective cross-sectional area and have a mass of less than 10 kg. The company, Tethers Unlimited, Inc. (TUI) has introduced the Terminator Tape, intended for use on small satellites, and it provides 10.5 m^2 area and has a mass of 0.808 kg [28]. Additionally, dragNET™ has a

mass of 2.8 kg and produces an area of 14 m^2 [25]. These designs and prototypes provide a baseline of what is possible for use on a midsized satellite.

This study focused on refining two of the requirements outlined by Rhatigan and Lan [3]. With respect to the drag area [3], "The drag area should be sufficient to de-orbit the spacecraft within 25 years using standard de-orbit calculation tools (e.g., STELA or DAS)." It was shown that 35 m^2 provides a practical drag area target for design and would de-orbit most of the satellites analyzed in this study, for altitudes less than 800 km. Another requirement from [3] addresses mass: "the mass of the de-orbit device should be minimized. A reasonable mass target is the mass of the propellant displaced for a de-orbit maneuver if the de-orbit device were not included." The 5 kg design target identified matches fuel offset in Table 10. This is supported by several flown examples and prototypes. Therefore, design targets of 5 kg mass and 35 m^2 area are practical to proceed to the next step of design for midsized satellites. All three of the drag device protypes could have had practical use with respect to satellites in this study; however, unique spacecraft would benefit most from a customized drag device as shown in Table 10. Therefore, either scalable and/or modular designs are desirable to tailor to specific spacecraft needs.

VI. CONCLUSIONS

A. SUMMARY

Based on the analysis of the satellites examined, drag devices are practical for self-disposal of many midsized satellites. The theoretical boundaries outlined by Rhatigan and Lan [3] were analyzed with a suite of existing spacecraft. It was found that the majority of midsized spacecraft in orbits below 800 km altitude could decay within 25 years with the inclusion of a drag device less than 35 m^2 as the sole method of self-disposal. Additionally, satellites above 800 km have the potential to reduce fuel mass if a drag enhancing device were to be used in combination with a perigee lowering maneuver. Of note, it was shown that more massive satellites have potential for higher mass savings and at higher orbital altitudes.

While there exist realistic limitations on how large a drag device can be, altitudes above 850 km are not practical as a sole method of self-disposal because of the dominant effects of SRP. Moreover, at 800 km, the area requirements to de-orbit with a sail alone become excessive. However, this study suggests that in conjunction with a propulsion burn, a drag device still provides mass savings for satellites beyond 800 km in altitude. The fuel mass savings ranged as high as 5.0 kg for IRS-P4 when used in conjunction with propulsion and using the "maximum" 35 m^2 drag device. If a modular device were to be used, potential fuel mass savings of 6.4 kg for OCO-2 can be seen. Conversely, there are scenarios wherein the introduction of a drag device would impose a cost in mass, and thus not be desirable. This occurs for CALIPSO if the mass of a drag device is assumed to be 5 kg. While this makes the use of a drag enhancing device less attractive for these satellites, the mass trade-off addresses only one aspect of its usefulness.

From a debris perspective, the biggest incentive to implementing drag enhancing devices is that they force compliance with the de-orbit requirements. They provide a single function and cannot be used to extend mission lifetime, as opposed to fuel reserved for de-orbit. For the spacecraft that could rely strictly on de-orbiting within 25 years from a drag device alone, there would be little to no risk of executing the planned de-orbit within

guidelines with a well-designed device. For the spacecraft that require propulsion regardless, the mass savings discussed in this study now provide an incentive with respect to mission lifetime.

The assumptions made throughout this study include estimations on spacecraft surface areas, generalizations of drag coefficients, estimated effective cross-sectional area and tumbling of satellites once defunct. As seen with the validation case studies, the ANDE satellites decayed sooner than the simulation estimated, even with a drag coefficient of 2 and a well-defined cross-sectional area. This "less conservative" estimation carried over when the case study satellites were examined, but it was less pronounced. Again, the drag coefficient was set at a value of 2, which is more conservative than normal satellite configurations [8]. This factor closely aligned the case study satellites' STELA simulations to their actual decay rates, when compared over the past decades of their EOL. The cross-sectional area simplification and tumbling assumptions are also estimates. It is likely that the "true" effective cross-sectional area that a drag device will produce will vary based on many factors. These include the rigidity of the device, where it is placed on the satellite, and how the shape of each satellite affects the interaction of aerodynamic forces. These factors are complex and unpredictable given the nature of the space solar environment.

B. FUTURE WORK

Many of the midsized LEO satellites in this study appear to be good candidates for the implementation of drag devices. Further analysis of more satellites in this class is one step to further validate that claim. Additionally, efforts should be made to investigate and identify future satellites that could be candidates for de-orbiting using a drag device. Analysis of satellites that have used drag devices, albeit smaller than the ones examined in this study, could also provide insight to their effectiveness.

Initially, hundreds of satellites were evaluated for study, but only twelve of them were analyzed in depth. Efforts were made to find a variety of different orbital regimes and satellite sizes and configurations, but the scope was nevertheless limited compared to what exists on orbit today. This is partially due to the sources available on satellite specifications, most of which came from the eoPortal. For this reason, many of the satellites were in sun-

synchronous orbits, which meant very similar inclinations and redundant altitudes. More data of actual spacecraft with a wider variety of orbital parameters would further clarify the problem statement addressed in this thesis.

Another area of recommended research is to investigate future satellites in a similar fashion to this study. The population of midsized satellites is expected to grow, according to [1]. An analysis of those future spacecraft would not only help to validate the potential for drag enhancing devices, but perhaps could identify candidates for their use. This study focused on existing satellites to determine "what could have happened if there were a drag device," because the data is available for both the satellite specifications and the orbit itself. However, applying this to planned orbits and spacecraft is a next step towards actual use of a drag device on a midsized satellite.

While there may not be much data on midsized satellites and drag enhancing devices, many smaller satellites have used such mechanisms. This data could be analyzed and compared to this study. Comparing the actual decay time to a model in STELA could clarify some of the assumptions that were made in this thesis. Notably, the Naval Postgraduate School (NPS) Spacecraft Architecture and Technology Demonstration Satellite, (NPSAT-1), recently deployed its tether drag device on 27 December 2020 [29]. NPSAT-1 is utilizing the TUI Terminator Tape, described in Chapter V, Section B. Although the drag device has only been in use for about six months, analysis of its performance is a topic of interest for further research.

THIS PAGE INTENTIONALLY LEFT BLANK

APPENDIX: CROSS-SECTIONAL AREA CALCULATIONS

$$Surface\ Area\ of\ Rectangular\ Prism(SA_r) = 2 \cdot (lw + hl + hw)$$
$$Surface\ Area\ of\ Cylinder\ (SA_c) = 2\pi rh + 2\pi r^2$$
$$Surface\ Area\ of\ Hexagonal\ Prism\ (SA_h) = 6sh + 3\sqrt{3} \cdot s^2$$
$$Total\ Surface\ Area = \ (SA_{bus}) + 2 \cdot Area\ of\ Solar\ Panel\ (for\ both\ sides)$$

Where *l = length, h = height, w = width, s = side length (hexagon), r = radius*

Table 10. Calculations for cross-sectional area determination

Name	**Solar Panel Number and Dimensions**	**Bus Dimensions (m)**	**Total Surface Area**	
CALIPSO	8 rectangular panels each 1.5 x 0.8 Source: [18]	Rectangular Prism (w, l, h) = (1.49,1.84, 2.31) Source [18]	$SA = 2 \cdot (1.49 \cdot 1.84 + 2.31 \cdot 1.84 + 2.31 \cdot 1.49)$ $+ 2 \cdot 8 \cdot (1.5 \cdot 0.8) = 40.13\ m^2$	$= \frac{40.13}{4}$ $= 10.0\ m^2$
CloudSat	6.4 m^2 Source: [18]	Rectangular Prism (w, l, h) = (2.3, 2.3, 2.8) Source [18]	$SA = 2 \cdot (2.3 \cdot 2.3 + 2.8 \cdot 2.3 + 2.8 \cdot 2.3)$ $+ 2 \cdot 6.4 = 49.1\ m^2$	$= \frac{49.1}{4}$ $= 12.3\ m^2$
F-3, F-6, F-7, F-11	9.2 m^2 Source: [17]	Cylinder $r = 0.75, h = 6.7$ Source [17]	$SA = 2\pi \cdot\ 0.75\ \cdot 6.7 + 2\pi . 75^2$ $+ 2 \cdot 9.2 = 53.5\ m^2$	$= \frac{53.5}{4}$ $= 13.4\ m^2$
EO-1	-	-	-	$6.03\ m^2$ Source [7]

FY-1A	2 rectangular panels each 3.5 x 1.2 Source [22]	Hexagonal Prism s =1.4, h =1.2 Source [22]	$SA = 6 \cdot 1.2 \cdot 1.4 + 3\sqrt{3} \cdot 1.4^2$ $+ 2 \cdot (2 \cdot 3.5 \cdot 1.2) = 37.1 m^2$	$= \frac{37.1}{4}$ $= 9.3\ m^2$
HY-1B	2 rectangular panels each 5.67 m^2 Source [19]	Rectangular Prism (w, l, h) = (1.4., 1.1, 0.953) Source [19]	$SA = 2 \cdot (1.4 \cdot 1.1 + 0.953 \cdot 1.4 + 0.953 \cdot 1.1)$ $+ 2 \cdot 2 \cdot (5.67) = 30.5\ m^2$	$= \frac{30.5}{4}$ $= 7.6\ m^2$
IRS-P4	2 rectangular panels each 9.6 m^2 Source [20]	Rectangular Prism (w, l, h) = (2.8, 1.98, 2.57) Source [20]	$SA = 2 \cdot (2.8 \cdot 1.98 + 2.57 \cdot 2.8 + 2.57 \cdot 1.98)$ $+ 2 \cdot 2 \cdot (9.6) = 74.1\ m^2$	$= \frac{74.1}{4}$ $= 18.5\ m^2$
OCO-2	2 rectangular panels each .47 x 2.12 Source [23]	Hexagonal Prism 0.94 $wide \rightarrow s$ =.47, h =2.12 Source [23]	$SA = 6 \cdot 2.12 \cdot .47 + 3\sqrt{3} \cdot .47^2$ $+ 2 \cdot (2 \cdot .47 \cdot 2.12) = 12.1 m^2$	$= \frac{12.1}{4}$ $= 3.0\ m^2$

LIST OF REFERENCES

[1] C. Palla and J. Kingston, "Forecast analysis on satellites that need de-orbit technologies: Future scenarios for passive de-orbit devices," *CEAS Space Journal* vol. 8, pp. 191–200, May 2016.

[2] K. Alsup et al., "Drag-Enhancing de-orbit devices for mid-sized spacecraft self-disposal," *IEEE*, March 02, 2019. [Online]. Available: https://ieeexplore.ieee.org/document/8741759

[3] J. Rhatigan and W. Lan, "Drag-enhancing de-orbit devices for spacecraft self-disposal: A review of progress and opportunities," *Journal of Space Safety Engineering,* vol. 7, no. 3, pp. 340–344, September 2020. [Online]. Available: https://www.sciencedirect.com/science/article/pii/S2468896720300896?via%3Dihub

[4] "Historical ELSET Search," space-track.org, February 1, 2021. [Online]. Available: https://www.space-track.org/

[5] U.S. Government, "U.S. Government orbital debris mitigation standard practices, November 2019 Update," November 2019. [Online]. Available: https://orbitaldebris.jsc.nasa.gov/library/usg_orbital_debris_mitigation_standard_practices_november_2019.pdf.

[6] *Orbital Debris Quarterly News*, NASA Orbital Debris Program Office, vol. 24, no. 1, February 2020.

[7] National Aeronautics and Space Administration. "End of Mission Plan for the Earth Observing-1 (EO-1) Satellite. Appendix B EO-1 Waiver, EO-1 Orbital Lifetime," 2007.

[8] D. Everett, J. Puschell, J. Wertz, *Space Mission Engineering: The New SMAD.* Portland, OR: Microcosm Press, 2011.

[9] B. Dunbar, "NASA's Nanosail-D 'Sails' Home—Mission Complete." NASA. November 29, 2011. [Online]. Available: https://www.nasa.gov/mission_pages/smallsats/11-148.html.

[10] K. Baker et al., "An updated re-entry analysis of the Hubble Space Telescope," *Journal of Space Safety Engineering*, vol. 7, no. 3, 2020, pp. 404–410, ISSN 2468–8967. [Online]. Available: https://www.sciencedirect.com/science/article/pii/S2468896720300707

[11] ESA Earth Observation Portal, eoPortal Directory, European Remote-Sensing Satellite-1. [Online]. Available: https://directory.eoportal.org/web/eoportal/satellite-missions/e/ers-1#footback9%29.

[12] CNES: STELA User's Guide, ver. 3.3 (2019).

[13] J. C. Liou, Debris Assessment Software User's Guide, Orbital Debris Program, NASA Johnson Space Center, Houston, Texas, May 2020.

[14] A. Nicholas, T. Fine, M. Davis, R. Kessel, "Atmospheric Neutral Density Experiment (ANDE-2) flight hardware details," May 26, 2009. Available: http://ilrs.gsfc.nasa.gov/docs/andehw.pdf

[15] C. Le Fèvre et al., "Compliance of disposal orbits with the French space operations act: The good practices and the STELA tool." *Acta Astronaut*, vol. 94, 234–245 (2014).

[16] G. Badhwar, P. Anz-Meador, "Determination of the area and mass distribution of orbital debris fragments." *Earth Moon Planet* 45, pp. 29–51 (1989). [Online]. Available: https://doi.org/10.1007/BF00054659

[17] ESA Earth Observation Portal, eoPortal Directory, Defense Meteorological Satellite Program Block 5D-3 Satellite Series [Online]. Available: https://directory.eoportal.org/web/eoportal/-/dmsp

[18] National Aeronautics and Space Administration, "CloudSat-CALIPSO launch, press kit," April 2006. [Online]. Available: http://www.nasa.gov/pdf/147741main_cloudsat-calipso4.pdf

[19] L. Wang, Z. Bai, "Practical CAST 968 platform used in HY-1B satellite," *Proceedings of the 59th IAC (International Astronautical Congress)*, Glasgow, Scotland, UK, Sept. 29 to Oct. 3, 2008, IAC-08.B4.3.11.

[20] ESA Earth Observation Portal, eoPortal Directory, OceanSat-1 – formerly IRS-P4 (Indian Remote Sensing Satellite -P4) [Online]. Available: https://directory.eoportal.org/web/eoportal/satellite-missions/i/irs-p4

[21] ESA Earth Observation Portal, eoPortal Directory, Ikonos-2 [Online]. Available: https://directory.eoportal.org/web/eoportal/satellite-missions/i/ikonos-2#foot5%29

[22] ESA Earth Observation Portal, eoPortal Directory, FY-1 (Feng Yun-1) [Online]. Available: https://directory.eoportal.org/web/eoportal/satellite-missions/f/fy-1

[23] ESA Earth Observation Portal, eoPortal Directory, OCO-2 (Orbiting Carbon Observatory-2) [Online]. Available: https://directory.eoportal.org/web/eoportal/satellite-missions/o/oco-2

[24] Y. Tsuda et al., “Flight status of IKAROS deep space solar sail demonstrator.” *Acta Astronautica*, vol. 69, no. 9–10, 2011, pp. 833–840.

[25] MMA Design, Dragnet™ De-Orbit System. [Online]. Available: https://mmadesignllc.com/product/dragnet-de-orbit-system/

[26] H. Kramer, “CanX-7 (Canadian Advanced Nanospace eXperiment-7),” EO, 2002. [Online]. Available: https://directory.eoportal.org/web/eoportal/satellite-missions/c-missions/canx-7

[27] S. Nichols, “De-orbiting drag sail,” M.S. thesis, Space Systems Academic Group, NPS, Monterey, CA, USA, 2020.

[28] Tethers Unlimited, “CubeSat terminator tape.” 2019. [Online]. Available: https://www.tethers.com/wp-content/uploads/2019/09/2019-Terminator-Tape.pdf

[29] J. Stroup, “NPSAT1: Assessment of risk for human casualty from atmospheric reentry,” M.S. thesis, Space Systems Academic Group, NPS, Monterey, CA, USA, March 2016.

THIS PAGE INTENTIONALLY LEFT BLANK

INITIAL DISTRIBUTION LIST

1. Defense Technical Information Center
   Ft. Belvoir, Virginia

2. Dudley Knox Library
   Naval Postgraduate School
   Monterey, California